Valley-Polarized Quantum Anomalous Hall State in Moiré math xmlns="http://www.w3.org/1998/Math/MathML" display="inline">mrow>msub>mrow>mi>MoTe/mi>/mrow>mrow>mn>2/mn>/mrow>/msub>mo>//mo>msub>mrow>mi>WSe/mi>/mrow>mrow>mn>2/mn>/mrow>/msub>/mrow>/math> Heterobilayers

Ying-Ming Xie, Cheng-Ping Zhang, Jin-Xin Hu, Kin Fai Mak, and K. T. Law

Phys. Rev. Lett. **128**, 026402 — Published 11 January 2022

DOI: 10.1103/PhysRevLett.128.026402

Theory of Valley Polarized Quantum Anomalous Hall State in Moiré $MoTe_2/WSe_2$ Heterobilayers

Ying-Ming Xie[1], Cheng-Ping Zhang[1], Jin-Xin Hu[1], Kin Fai Mak[2,3,4], and K. T. Law[1*]
[1]*Department of Physics, Hong Kong University of Science and Technology, Clear Water Bay, Hong Kong, China*
[2]*School of Applied and Engineering Physics, Cornell University, Ithaca, NY, USA*
[3]*Kavli Institute at Cornell for Nanoscale Science, Ithaca, NY, USA and*
[4]*Laboratory of Atomic and Solid State Physics, Cornell University, Ithaca, NY, USA*
(Dated: December 22, 2021)

Moiré heterobilayer transition metal dichalcogenides (TMDs) emerge as an ideal system for simulating the single-band Hubbard model and interesting correlated phases have been observed in these systems. Nevertheless, the moiré bands in heterobilayer TMDs were believed to be topologically trivial. Recently, it was reported that both a quantum valley Hall insulating state at filling $\nu = 2$ (two holes per moiré unit cell) and a valley polarized quantum anomalous Hall state at filling $\nu = 1$ were observed in AB stacked moiré $MoTe_2/WSe_2$ heterobilayers. However, how the topologically nontrivial states emerge is not known. In this work, we propose that the pseudo-magnetic fields induced by lattice relaxation in moiré $MoTe_2/WSe_2$ heterobilayers could naturally give rise to moiré bands with finite Chern numbers. We show that a time-reversal invariant quantum valley Hall insulator is formed at full-filing $\nu = 2$, when two moiré bands with opposite Chern numbers are filled. At half-filling $\nu = 1$, Coulomb interaction lifts the valley degeneracy and results in a valley polarized quantum anomalous Hall state, as observed in the experiment. Our theory identifies a new way to achieve topologically non-trivial states in heterobilayer TMD materials.

Introduction.— Recently, there is an intense study on the moiré superlattices such as in twisted bilayer graphene [1–10] and twisted bilayer transition metal dichalcogenides (TMDs) [11–29]. The narrow moiré bands together with strong electron-electron interactions give rise to various interesting quantum states of matter.

The moiré superlattices formed by TMD heterobilayers are particularly interesting [16–30]. A moiré TMD heterobilayer is formed by stacking two different 2H-structure monolayer TMDs MX_2 and $\tilde{M}\tilde{X}_2$. Due to the large energy offset of the valence bands of the two TMDs, the electrons near the Fermi energy are mostly originated from the TMD layer with higher valence band energy. Therefore, a moiré TMD heterobilayer can be approximately treated as a monolayer TMD with an additional moiré potential which is created through interlayer couplings. Moreover, due to the large Ising spin-orbit coupling [31–33], spin degeneracy is lifted while the valley degeneracy plays the role of pseudo-spin. In the presence of Coulomb interactions, a moiré TMD heterobilayer can be treated as a single-band Hubbard model simulator [18, 23] with parameters highly tunable through the twist angle and the displacement field. Several interesting correlated phenomena such as Mott insulating states[23], Wigner crystal states[24], Pomeranchuk effect and continuous Mott transition [29] have been observed in AA stacked moiré TMD heterobilayers. However, so far the moiré bands in heterobilayers are expected to be topologically trivial and topology does not play a role in these correlated phases.

Surprisingly, in a recent experiment with AB stacked moiré $MoTe_2/WSe_2$ heterobilayers, a quantum valley Hall insulator state at full-filling $\nu = 2$, i.e., two holes per moiré unit cell, and a quantum anomalous Hall state at half-filling $\nu = 1$ were observed [34]. As the quantized Hall resistance strongly correlates with valley polarization through magnetic circular dichroism measurements, it is strongly suggestive that the quantum anomalous Hall state is a valley polarized anomalous Hall state[34]. Although it was predicted that the quantum valley Hall state can emerge in homobilayer TMDs [14] which can be described by a Kane-Mele model [35], the low energy description of heterobilayers is dramatically different due to the large offset of the energy of the bands which is estimated to be around 300 meV [29, 34] and large differences in interlayer tunnelling strengthens. Therefore, the origin of the topologically non-trivial bands in heterobilayers is not known.

In this work, we point out that a periodically modulated pseudo-magnetic field, which could emerge spontaneously under lattice relaxation, can give rise to topologically nontrivial moiré bands. Specifically, (i) the pseudo-magnetic field can create Chern bands with opposite Chern numbers at opposite valleys. As a result, a quantum valley Hall insulating phase would form at $\nu = 2$, when the topmost moiré bands at two valleys are filled; (ii) Importantly, at half-filling $\nu = 1$, based on a self-consistent Hartree-Fock calculation, we found the Coulomb interactions could lift the degeneracies of the two valleys. It results in an interactions-driven valley polarized quantum anomalous Hall phase as observed in the recent experiments. Our theory identifies a new way to achieve topologically non-trivial states in heterobilayer TMD materials which were considered topologically trivial.

Model.— As pointed out in Ref. [18], due to the large Ising spin-orbit coupling which breaks the spin-degeneracy and the layer asymmetry, a TMD heterobilayer can be described by a single-band Hubbard model

with the valley degrees of freedom playing the role of pseudo-spins. However, the resulting moiré bands are topologically trivial. One important element which was not considered in the original model of TMD heterobilayer [18] is lattice relaxation. Indeed, it has been shown that local strain can result in lattice relaxation and even lattice reconstructions which are important in twisted bilayer graphene [36, 37] and twisted TMDs [38–43]. Importantly, the lattice relaxation can generate periodically modulated pseudo-magnetic fields which play an important role in the moiré band structure [36].

To capture the effects of periodic pseudo-magnetic fields $B(\boldsymbol{r})$, we include an additional gauge field $\boldsymbol{A}$ with $B(\boldsymbol{r}) = \nabla \times \boldsymbol{A}(\boldsymbol{r})$ into the previously proposed model Hamiltonian for the moiré TMD heterobilayer [18, 27] as $H = \int d\boldsymbol{r}\psi_\tau^\dagger(\boldsymbol{r})\mathcal{H}_\tau(\boldsymbol{r})\psi_\tau(\boldsymbol{r})$. Here,

$$\mathcal{H}_\tau(\boldsymbol{r}) = -\frac{(\hat{\boldsymbol{p}} + \tau e\boldsymbol{A})^2}{2m^*} + V(\boldsymbol{r}), \tag{1}$$

where the momentum operator $\hat{\boldsymbol{p}} = -i\hbar\nabla$, m^* is the valence band effective mass, $\tau = \pm$ for $\pm K$ valley. The moiré potential is $V(\boldsymbol{r}) = 2V_0\sum_{j=1,3,5}\cos(\boldsymbol{G}_j \cdot \boldsymbol{r} + \phi)$ with moiré wave vectors $\boldsymbol{G}_j = \frac{4\pi}{\sqrt{3}L_M}(\cos(\frac{(j-1)\pi}{3}), \sin(\frac{(j-1)\pi}{3}))$, $L_M \approx a/\sqrt{\delta^2+\theta^2}$ is the moiré lattice constant with a lattice constant mismatch $\delta = (a-a')/a$ and a twist angle θ. To be specific, we adopted the parameters: $m^* = 0.6m_0$ with m_0 the electron mass, $a = 3.565$Å, $a' = 3.317$Å [44–46] for the band structure calculations of TMD $MoTe_2/WSe_2$ heterobilayers, where the top valence moiré bands originate from $MoTe_2$ layer [29, 34]. The model Hamiltonian H respects C_3 symmetry and time-reversal symmetry $T = \tau_x\hat{K}$ with $\hat{K}$ as complex conjugate operation, and the moiré Hamiltonians of the two valleys are related by time-reversal symmetry: $T\mathcal{H}_\tau(\boldsymbol{r})T^{-1} = \mathcal{H}_{-\tau}(\boldsymbol{r})$.

We first consider the case without the pseudo-magnetic fields $B(\boldsymbol{r})$, i.e., $\boldsymbol{A} = 0$, the moiré Hamiltonian exhibits a spinless time-reversal symmetry: $T'\mathcal{H}_\tau(\boldsymbol{r})T'^{-1} = \mathcal{H}_\tau(\boldsymbol{r})$ with $T' = \hat{K}$. This spinless time-reversal symmetry enforces the Berry curvature to be an odd function: $\Omega(\boldsymbol{k}) = -\Omega(-\boldsymbol{k})$ (Supplementary Material (SM) Sec. I[47]). As a result, the Chern number of each moiré band is zero. To break this spinless time-reversal symmetry, an additional periodically modulated pseudo-magnetic field $\boldsymbol{B}$ is introduced in the moiré Hamiltonian (1). Evidently, in this case $T'\mathcal{H}_\tau(\boldsymbol{r})T'^{-1} \neq \mathcal{H}_\tau(\boldsymbol{r})$. Hence, moiré bands with finite Chern numbers are allowed.

To be specific, we consider a C_3-invariant periodic pseudo-magnetic field: $B(\boldsymbol{r}) = B_0\sum_{j=1,3,5}\cos(\boldsymbol{G}_j \cdot \boldsymbol{r})$, which is expected to emerge in an AB stacked moiré TMD bilayer under lattice relaxation as shown in Ref. [38] or can be generated by some out of plane corrugation effects [54, 55]. The topography of this pseudo-magnetic field is shown in Fig. 1(a). It displays the same period as the moiré superlattice, and it is important to note that the

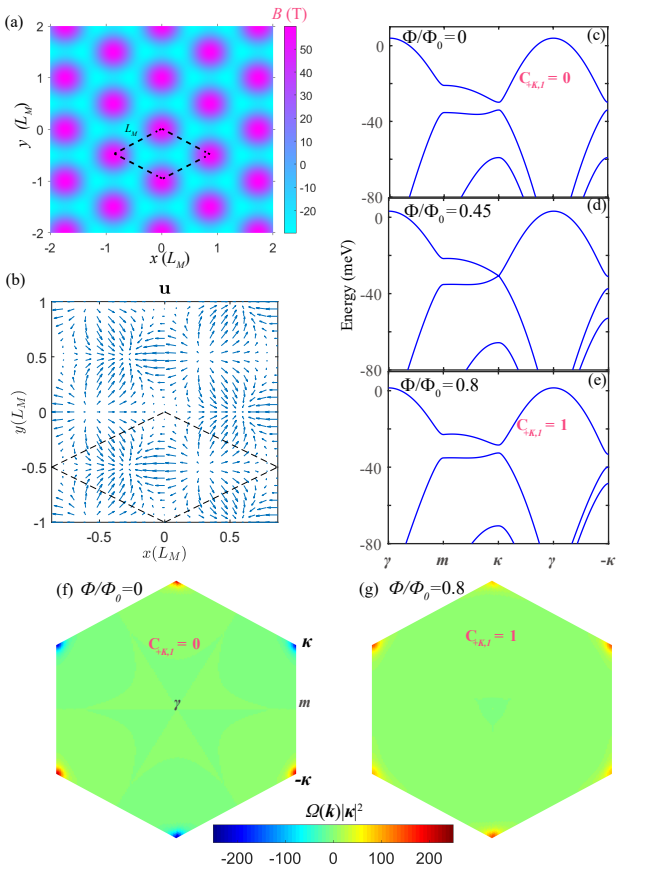

FIG. 1: (a) and (b) show the topography of a C_3 symmetric periodic pseudo-magnetic field ($B_0 = 20$T) and the corresponding strain displacement field $\boldsymbol{u}$, respectively. (c), (d) and (e) show the moiré band structures at valley K calculated at $\Phi/\Phi_0 = 0, 0.45, 0.8$ respectively, where the moiré potential parameters are taken as $V_0 = 10$ meV, $\phi = 0.3\pi$, $\theta = 0.53°$. The top two moiré bands at Φ/Φ_0 with Chern number $C_{K,1}$ and $C_{K,2}$ are highlighted. The corresponding distributions of the Berry curvature within moiré Brillouin zone at $\Phi/\Phi_0 = 0$ and $\Phi/\Phi_0 = 0.8$ are shown in (f) and (g), respectively.

net flux in each moiré unit cell is zero, as we will see later the topology of this system can be understood in terms of the Haldane model [56]. The corresponding gauge field of $B(\boldsymbol{r})$ is derived as $\boldsymbol{A}(\boldsymbol{r}) = A_0[\boldsymbol{a_2}\sin(\boldsymbol{G_1}\cdot\boldsymbol{r}) - \boldsymbol{a_1}\sin(\boldsymbol{G_3}\cdot\boldsymbol{r}) - \boldsymbol{a_3}\sin(\boldsymbol{G_5}\cdot\boldsymbol{r})]$, where $\boldsymbol{a_1} = (\frac{\sqrt{3}}{2}, \frac{1}{2})L_M$, $\boldsymbol{a_2} = (0,1)L_M$, $\boldsymbol{a_3} = \boldsymbol{a_2} - \boldsymbol{a_1}$, and $A_0 = \sqrt{3}B_0/4\pi$. This gauge field can be generated by a two-dimensional strain field $u_{ij}(\boldsymbol{r}) = (\partial_i u_j(\boldsymbol{r}) + \partial_j u_i(\boldsymbol{r}))/2$ [54, 57, 58] with $\boldsymbol{A} = \alpha(2u_{xy}, u_{xx} - u_{yy})$. The strain displacement field that gives rise to the periodic $B(\boldsymbol{r})$ is plotted in Fig. 1(b) (see the detail in Supplementary Material(SM)[47]). The periodic strain displacement has been observed in moiré TMD bilayers [41–43]. Physically, there are different types of local stacking configurations which result in different lattice relaxation within a moiré unit cell [38, 47]. As presented in SM [47] such lattice relaxation could gen-

erate the periodic pseudomagnetic fields we introduced.

Inserting $\boldsymbol{A}(\boldsymbol{r})$ into Eq. (1), we obtained $\mathcal{H}_\tau(\boldsymbol{r}) = -\frac{(\hat{\boldsymbol{p}}+\tau\frac{\Phi}{\Phi_0}\tilde{\boldsymbol{A}})^2}{2m^*} + V(\boldsymbol{r})$, where $\Phi_0 = \frac{h}{e}$ is a flux quantum and $\Phi = \frac{\sqrt{3}}{2}B_0 L_M^2$ has the dimension of magnetic flux, $\tilde{\boldsymbol{A}} = \frac{4\pi \boldsymbol{A}(\boldsymbol{r})}{\sqrt{3}B_0 L_M^2}$. We can then diagonalize $\mathcal{H}_\tau(\boldsymbol{r})$ with plane wave basis to obtain the moiré bands (SM Sec. IVA [47]).

As an illustration, in Fig. 1(c) to (e), we show the energy spectrum of $+K$ valley ($\tau = +1$) at a commensurate angle $\theta = 0.53°$ [27] but with different strength of pseudo-magnetic field: $\Phi/\Phi_0 = 0, 0.45, 0.8$. The corresponding Berry curvature distribution of top moiré bands at $\Phi/\Phi_0 = 0$ and $\Phi/\Phi_0 = 0.8$ are shown in Fig. 1(f) and Fig. 1(g). Without the pseudo-magnetic field, the moiré band carries zero Chern number (labeled in Fig. 1(c)), although there appears to be finite Berry curvature at moiré Brillouin zone corners $\pm\kappa$ (Fig. 1(f)). With an increase in the pseudo-magnetic field, it can be seen that the gap at κ is closed at $\Phi/\Phi_0 = 0.45$ and reopens when $\Phi/\Phi_0 > 0.45$, which results in finite Chern numbers for the top two moiré bands (labeled in Fig. 1(e)). It is clear from Fig. 1(g) that, for the band with a finite Chern number, the Berry curvature has the same sign in the whole Brillouin zone.

Topological phase diagram.—To understand the topological phase transition, we derived an effective Hamiltonian near $\pm\kappa$ by performing perturbation theory at three moiré Brillouin corners connected by the reciprocal lattice vectors for the moiré pattern (SM Sec. IIA [47]). The resulting effective Hamiltonian is

$$H^{eff}_{\pm\kappa}(\boldsymbol{k}) = \begin{pmatrix} \epsilon_0 + 2V_0\cos\phi & \pm\frac{1}{2}v(k_x + ik_y) & \pm\frac{1}{2}v(k_x - ik_y) \\ \pm\frac{1}{2}v(k_x - ik_y) & \epsilon_0 + 2V_0\cos(\frac{2\pi}{3}+\phi) \mp \epsilon_B & \pm\frac{1}{2}v(k_x + ik_y) \\ \pm\frac{1}{2}v(k_x + ik_y) & \mp\frac{i}{2}v(k_x - ik_y) & \epsilon_0 + 2V_0\cos(\frac{4\pi}{3}+\phi) \pm \epsilon_B \end{pmatrix}, \tag{2}$$

where $\boldsymbol{k}$ is expanded near $\pm\kappa$, $\epsilon_0 = -\kappa^2/2m^*$, $v = \kappa/m^*$, $\epsilon_B = \frac{\sqrt{3}v}{4L_M}\frac{\Phi}{\Phi_0} = \frac{\hbar e B_0}{4m^*}$ is a magnetic energy due to the presence of pseudo-magnetic fields. Interestingly, this three-band Hamiltonian exhibits as a Dirac Hamiltonian at every two-band subspace. Moreover, the ϵ_B shifts the Dirac mass in opposite way at $+\kappa$ and $-\kappa$. This feature maps the effective Hamiltonian back to the Haldane model [56] and moiré bands with finite Chern number would thus be created when the Dirac mass term changes sign at $+\kappa$ or $-\kappa$. The topological phase transition boundary lines are obtained as:

$$L_1 : \frac{\epsilon_B}{V_0} = \pm 2[\cos(\frac{2\pi}{3}+\phi) - \cos\phi]; \tag{3}$$

$$L_2 : \frac{\epsilon_B}{V_0} = \pm 2[\cos\phi - \cos(\frac{4\pi}{3}+\phi)]; \tag{4}$$

$$L_3 : \frac{\epsilon_B}{V_0} = \pm[\cos(\frac{2\pi}{3}+\phi) - \cos(\frac{4\pi}{3}+\phi)]. \tag{5}$$

Surprisingly, the topological phase transition boundary lines L_j only rely on the ratio $\frac{\epsilon_B}{V_0}$ and the phase ϕ of the moiré potential in the perturbative regime, where the moiré bandwidth ϵ_W is much larger than the magnetic energy ϵ_B.

To determine the possible nontrivial topological regions, the Chern number C of the top moiré band with various ϕ and ratio ϵ_B/V_0 is calculated numerically (SM Sec. IVB [47]). The typical topological phase diagram within ($V_0 = 1$ meV) and beyond ($V_0 = 10$ meV) the perturbation region are displayed in Fig. 2(a) and Fig. 2(b), respectively, where C is found to be able to take the value of 0, ±1 and ±2. The phase boundaries given by the effective Hamiltonian (2) are also depicted in Fig. 2 as red dashed lines. In Fig. 2(a), impressively, most of the phase boundaries in numerical results match the results from the effective Hamiltonian. As shown in Fig. 2(b), the phase boundaries become more complicated beyond the perturbative regime. Nevertheless, there is still a large proportion of parameter space that exhibits Chern number $C = \pm1$.

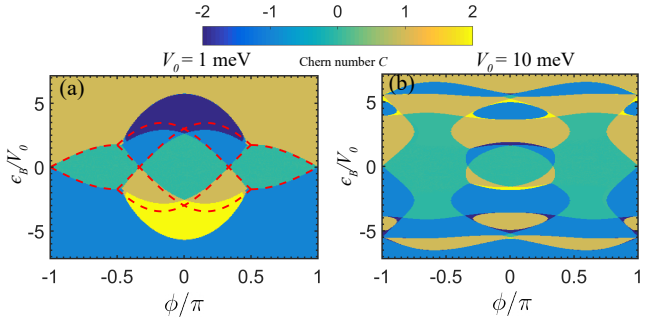

FIG. 2: (a) and (b) respectively, display the Chern number C as a function of phase ϕ and the strength of the pseudo-magnetic fields characterized by the ratio of ϵ_B/V_0 with $V_0 = 1$ meV and $V_0 = 10$ meV. The red dashed lines represent the phase boundaries given by the effective Hamiltonian.

We now discuss the accessibility of parameter space with finite Chern numbers. As shown in Fig. 2, the optimal ϕ is near $\pi/3$ and π, and a large magnetic energy ϵ_B at the order of V_0 is desired. Note that the magnitude of $\epsilon_B = \frac{\hbar e B_0}{4m^*} \sim 0.05 B_0$ meV/T is determined by the strength of pseudo-magnetic fields B_0. Considering a B_0

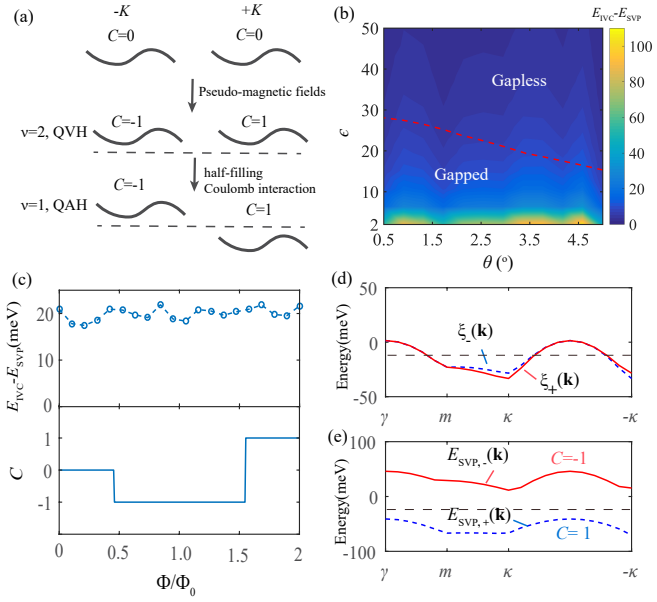

FIG. 3: (a) Schematic plot of the evolution of Chern number for top moiré bands at two valleys in the presence of pseudo-magnetic fields, different fillings and interaction with the emergence of quantum valley Hall (QVH) at filling $\nu = 2$ and valley polarized quantum anomalous Hall (QAH) at filling $\nu = 1$. (b) The energy difference between the inter-valley coherent state (IVC) and the spin-valley-polarized (SVP) state: $E_{IVC} - E_{SVP}$ (in units of meV) as a function of dielectric constant ϵ and twist angle θ. (c) shows the evolution of $E_{IVC} - E_{SVP}$ (top panel) and Chern number (lower panel) at finite flux. (d) and (e), respectively, show the moiré band structures $\xi_\tau(\boldsymbol{k})$ and the mean-field band structures of the SVP state $E_{SVP,\tau}(\boldsymbol{k})$ at $\Phi/\Phi_0 = 0.8$. The parameters for moiré potential in (b) to (e) are taken as $V_0 = 10$ meV $\phi = 0.3\pi$, $\theta = 0.53°$. Here, $\epsilon = 10$, $\lambda^{-1} = 10$ nm [11, 29, 59] are adopted for (c) to (e).

of tens of T, the magnetic energy ϵ_B is estimated to be several meV which is achievable in heterobilayer TMDs and other moiré materials [38]. As shown in Fig. 2, this ϵ_B is certainly sufficient to drive the system to be topological for ϕ near $\pi/3$ and π, while for ϕ far from these regions, it would depend on the magnitude of V_0. A large V_0 would tend to make the system trivial since it would enhance the trivial energy gap between moiré bands. In the case of a large V_0 (tens of meVs), the topological region may still be achievable through a displacement field [29], because the displacement field effectively tunes the interlayer tunneling so that V_0 could be effectively changed.

Valley polarized quantum anomalous Hall states at half-filling $\nu = 1$.—After demonstrating the formation of Chern bands in moiré TMD heterobilayers with periodic pseudo-magnetic fields, we now study the interaction induced topological phases, as schematically depicted in Fig. 3(a). We consider the case where the Chern number $C = \pm 1$ at the $\pm K$ valley. Due to the spin-valley locking, the moiré TMD heterobilayer is a quantum valley Hall insulating phase at the full-filling $\nu = 2$ (see Fig. 3(a)). When the chemical potential is tuned to half-filling $\nu = 1$, as we will demonstrate later, the Coulomb interaction could lift the valley degeneracy and thus gives rise to a valley polarized quantum anomalous Hall insulator.

In moiré TMD heterobilayer, due to the spin-valley locking, the Coulomb interaction is simply

$$H_{int} = \frac{1}{2S}\sum_{\boldsymbol{k},\boldsymbol{k'},\boldsymbol{q}} V(\boldsymbol{q}) c^\dagger_\tau(\boldsymbol{k}+\boldsymbol{q}) c^\dagger_{\tau'}(\boldsymbol{k'}-\boldsymbol{q}) c_{\tau'}(\boldsymbol{k'}) c_\tau(\boldsymbol{k}), \tag{6}$$

where S is the sample area, $V(\boldsymbol{q}) = \frac{e^2}{2\epsilon\epsilon_0\sqrt{q^2+\lambda^2}}$ is the screened Coulomb interaction with ϵ, ϵ_0, λ^{-1} denoting the dielectric constant, vacuum permittivity and a screened length. In practice, the dielectric constant and screened length are determined by the surrounding hBN and metallic gates [60]. Within the Hartree-Fock mean-field analysis, we define the order parameter as $\langle\psi_G|c^\dagger_\tau(\boldsymbol{k})c_{\tau'}(\boldsymbol{k'})|\psi_G\rangle = \Delta_{\tau\tau'}(\boldsymbol{k})\delta_{\boldsymbol{k},\boldsymbol{k'}}$, where $|\psi_G\rangle$ denotes the ground state. Unlike moiré superlattices of graphene [9, 59, 61–63], here due to the spin-valley locking, the possible gapped correlated ground states for moiré TMD heterobilayer can be simply grouped into two categories at half-filling: (i) the spin-valley-polarized (SVP) state $|\psi_G\rangle = \Pi_{|\boldsymbol{k}|<k_F} c^\dagger_\tau(\boldsymbol{k})|0\rangle$, where only τ-valley is occupied; (ii) the spin-valley-locked intervalley coherent (IVC) state $|\psi_G\rangle = \Pi_{|\boldsymbol{k}|<k_F}[\sin\frac{\theta_{\boldsymbol{k}}}{2}e^{-i\frac{\varphi_{\boldsymbol{k}}}{2}}c^\dagger_+(\boldsymbol{k}) + \cos\frac{\theta_{\boldsymbol{k}}}{2}e^{i\frac{\varphi_{\boldsymbol{k}}}{2}}c^\dagger_-(\boldsymbol{k})]|0\rangle$, where $\theta_{\boldsymbol{k}} = \pi - \theta_{-\boldsymbol{k}}$ and $\varphi_{\boldsymbol{k}} = \varphi_{-\boldsymbol{k}}$ to preserve the time-reversal symmetry. The SVP state breaks time-reversal symmetry, while the spin-valley-locked IVC state breaks the $U(1)$ valley-charge conservation. Importantly, as a result of a single valley occupancy, a SVP ground state at half-filling $\nu = 1$ could lead to the valley polarized quantum anomalous Hall insulating state.

To study the stabilized ground state at $\nu = 1$, we performed the Hartree-Fock mean-field calculations. In the calculations, we projected the interactions onto the topmost moiré bands [9, 61, 62]. The details of the calculations can be found in SM Sec. III and Sec. IV [47]. Here, we summarize the numerical results in Fig. 3(b) to Fig. 3(f). Fig. 3(b) displays the energy difference of the IVC and SVP state $E_{IVC} - E_{SVP}$ as a function of twist angle θ and dielectric constant ϵ. It is shown that in a wide parameter range, the SVP state exhibits lower energy than the IVC state, being compatible with previous results in moiré superlattices of graphene [61, 62, 64]. Indeed, $E_{IVC} - E_{SVP} > 0$ can be shown analytically in the long-wave limit $qL_M \ll 1$ as shown in SM Sec. III [47]. To obtain the observed insulating QAH state, a gapped SVP state is needed, which happens when the strength of Coulomb interaction overcomes the band dispersion as highlighted in Fig. 3(b).

We also performed the Hartree-Fock mean-field calculations with finite pseudo-magnetic fields ($\Phi = \frac{\sqrt{3}}{2} B_0 L_M^2 \neq 0$) which enables the moiré bands to carry finite Chern numbers. We found that the SVP state is still more stable than the IVC state in this case. As shown in the upper panel of Fig. 3(c), the energy difference of $E_{IVC} - E_{SVP}$ is almost insensitive to the increase in the strength of pseudo-magnetic fields. This is because the corresponding magnetic energy ϵ_B is much smaller than the Coulomb interacting strength ($\sim$ 100 meV). In contrast with the stability of the SVP state, the topology of the moiré bands is determined by specific pseudo-magnetic fields. As shown in the lower panel of Fig. 3(c), the SVP states acquired finite Chern numbers at some range of pseudo-magnetic fields. Therefore, by considering the effects of pseudo-magnetic fields and Coulomb interactions, we demonstrated the degeneracy of the two moiré bands $\xi_{\pm}(\boldsymbol{k})$ can be lifted (see Fig. 3(d)) and a single moiré band carrying a finite Chern number appears at half-filling (see Fig. 3(e)). As a result, moiré TMD heterobilayers can exhibit valley polarized quantum anomalous Hall states.

Discussion.— It is important to note that another natural way to create nontrivial Chern bands is by reducing the energy offset of the valence bands of $MoTe_2$ and WSe_2 by applying a displacement field, such that the moiré bands of the two TMD materials can hybridize to open a topologically non-trivial gap [14, 55]. However, it is not certain if the relatively small displacement field ($\sim$0.5 V/nm) used in the experiment [34] can hybridize the moiré bands from $MoTe_2$ and WSe_2, which are expected to have an energy offset of 300meV [29, 34]. In the case of QAH effect observed at 3/4 filling in twisted bilayer graphene, the non-trivial Chern bands are generated by the coupling between the aligned graphene moiré superlattices and the boron nitride substrate [4, 7, 61, 65–67]. In this work, we propose a new mechanism that pseudo-magnetic fields induced by lattice relaxation can cause topological band inversion for moiré bands originated from a single layer (such as the $MoTe_2$ layer). Our results in principle can be applicable to other TMD materials with pseudo-magnetic fields [38, 54, 68]. Our model also provides a basis for the study of other strongly interacting phases such as fractional Chern insulating states [69–72] in heterobilayer TMDs.

In the SM Sec. V [47], we go beyond the pseudo-magnetic field approximation and introduce an effective tight-binding model to describe the $MoTe_2/WSe_2$ heterobilayer with lattice relaxation. We demonstrate how lattice relaxation can cause gap closing and reopening and change the topology of the top moiré bands. Both the gap closing positions as well as the topology of bands of the effective tight-binding model are consistent with the results from the pseudomagnetic field description.

Acknowledgments.— The authors thank the discussions with Liang Fu, Adrian Po, and Berthold Jäck. K.T.L. acknowledges the support of the Croucher Foundation and HKRGC through RFS2021-6S03, C6025-19G, AoE/P-701/20, 16310520, 16310219 and16309718. K.F.M. acknowledges the support of the Air Force Office of Scientific Research under award number FA9550-20-1-0219.

* Corresponding author.
phlaw@ust.hk

[1] Y. Cao, V. Fatemi, A. Demir, S. Fang, S. L. Tomarken, J. Y. Luo, J. D. Sanchez-Yamagishi, K. Watanabe, T. Taniguchi, E. Kaxiras, R. C. Ashoori, and P. Jarillo-Herrero, Nature **556**, 80 (2018).
[2] Y. Cao, V. Fatemi, S. Fang, K. Watanabe, T. Taniguchi, E. Kaxiras, and P. Jarillo-Herrero, Nature **556**, 43 (2018).
[3] M. Yankowitz, S. Chen, H. Polshyn, Y. Zhang, K. Watanabe, T. Taniguchi, D. Graf, A. F. Young, and C. R. Dean, Science **363**, 1059 (2019).
[4] A. L. Sharpe, E. J. Fox, A. W. Barnard, J. Finney, K. Watanabe, T. Taniguchi, M. A. Kastner, and D. Goldhaber-Gordon, Science **365**, 605 (2019).
[5] A. Kerelsky, L. J. McGilly, D. M. Kennes, L. Xian, M. Yankowitz, S. Chen, K. Watanabe, T. Taniguchi, J. Hone, C. Dean, A. Rubio, and A. N. Pasupathy, Nature **572**, 95 (2019).
[6] Y. Xie, B. Lian, B. Jäck, X. Liu, C.-L. Chiu, K. Watanabe, T. Taniguchi, B. A. Bernevig, and A. Yazdani, Nature **572**, 101 (2019).
[7] M. Serlin, C. L. Tschirhart, H. Polshyn, Y. Zhang, J. Zhu, K. Watanabe, T. Taniguchi, L. Balents, and A. F. Young, Science **367**, 900 (2020).
[8] R. Bistritzer and A. H. MacDonald, Proceedings of the National Academy of Sciences **108**, 12233 (2011).
[9] H. C. Po, L. Zou, A. Vishwanath, and T. Senthil, Phys. Rev. X **8**, 031089 (2018).
[10] M. Koshino, N. F. Q. Yuan, T. Koretsune, M. Ochi, K. Kuroki, and L. Fu, Phys. Rev. X **8**, 031087 (2018).
[11] L. Wang, E.-M. Shih, A. Ghiotto, L. Xian, D. A. Rhodes, C. Tan, M. Claassen, D. M. Kennes, Y. Bai, B. Kim, K. Watanabe, T. Taniguchi, X. Zhu, J. Hone, A. Rubio, A. N. Pasupathy, and C. R. Dean, Nature Materials **19**, 861 (2020).
[12] Z. Zhang, Y. Wang, K. Watanabe, T. Taniguchi, K. Ueno, E. Tutuc, and B. J. LeRoy, Nature Physics **16**, 1093 (2020).
[13] M. H. Naik and M. Jain, Phys. Rev. Lett. **121**, 266401 (2018).
[14] F. Wu, T. Lovorn, E. Tutuc, I. Martin, and A. H. MacDonald, Phys. Rev. Lett. **122**, 086402 (2019).
[15] Z. Bi and L. Fu, Nature Communications **12**, 642 (2021).
[16] C. Zhang, C.-P. Chuu, X. Ren, M.-Y. Li, L.-J. Li, C. Jin, M.-Y. Chou, and C.-K. Shih, Science Advances **3** (2017), 10.1126/sciadv.1601459.
[17] Q. Tong, H. Yu, Q. Zhu, Y. Wang, X. Xu, and W. Yao, Nature Physics **13**, 356 (2017).
[18] F. Wu, T. Lovorn, E. Tutuc, and A. H. MacDonald, Phys. Rev. Lett. **121**, 026402 (2018).
[19] C. Jin, E. C. Regan, A. Yan, M. Iqbal Bakti Utama, D. Wang, S. Zhao, Y. Qin, S. Yang, Z. Zheng, S. Shi,

K. Watanabe, T. Taniguchi, S. Tongay, A. Zettl, and F. Wang, Nature **567**, 76 (2019).
[20] K. Tran, G. Moody, F. Wu, X. Lu, J. Choi, K. Kim, A. Rai, D. A. Sanchez, J. Quan, A. Singh, J. Embley, A. Zepeda, M. Campbell, T. Autry, T. Taniguchi, K. Watanabe, N. Lu, S. K. Banerjee, K. L. Silverman, S. Kim, E. Tutuc, L. Yang, A. H. MacDonald, and X. Li, Nature **567**, 71 (2019).
[21] K. L. Seyler, P. Rivera, H. Yu, N. P. Wilson, E. L. Ray, D. G. Mandrus, J. Yan, W. Yao, and X. Xu, Nature **567**, 66 (2019).
[22] Y. Shimazaki, I. Schwartz, K. Watanabe, T. Taniguchi, M. Kroner, and A. Imamoğlu, Nature **580**, 472 (2020).
[23] Y. Tang, L. Li, T. Li, Y. Xu, S. Liu, K. Barmak, K. Watanabe, T. Taniguchi, A. H. MacDonald, J. Shan, and K. F. Mak, Nature **579**, 353 (2020).
[24] E. C. Regan, D. Wang, C. Jin, M. I. Bakti Utama, B. Gao, X. Wei, S. Zhao, W. Zhao, Z. Zhang, K. Yumigeta, M. Blei, J. D. Carlström, K. Watanabe, T. Taniguchi, S. Tongay, M. Crommie, A. Zettl, and F. Wang, Nature **579**, 359 (2020).
[25] Y. Xu, S. Liu, D. A. Rhodes, K. Watanabe, T. Taniguchi, J. Hone, V. Elser, K. F. Mak, and J. Shan, Nature **587**, 214 (2020).
[26] X. Huang, T. Wang, S. Miao, C. Wang, Z. Li, Z. Lian, T. Taniguchi, K. Watanabe, S. Okamoto, D. Xiao, S.-F. Shi, and Y.-T. Cui, Nature Physics **17**, 715 (2021).
[27] Y. Zhang, N. F. Q. Yuan, and L. Fu, Phys. Rev. B **102**, 201115 (2020).
[28] C. Jin, Z. Tao, T. Li, Y. Xu, Y. Tang, J. Zhu, S. Liu, K. Watanabe, T. Taniguchi, J. C. Hone, L. Fu, J. Shan, and K. F. Mak, Nature Materials (2021), 10.1038/s41563-021-00959-8.
[29] T. Li, S. Jiang, L. Li, Y. Zhang, K. Kang, J. Zhu, K. Watanabe, T. Taniguchi, D. Chowdhury, L. Fu, J. Shan, and K. F. Mak, Nature **597**, 350 (2021).
[30] N. Morales-Durán, A. H. MacDonald, and P. Potasz, Phys. Rev. B **103**, L241110 (2021).
[31] D. Xiao, G.-B. Liu, W. Feng, X. Xu, and W. Yao, Phys. Rev. Lett. **108**, 196802 (2012).
[32] X. Xi, Z. Wang, W. Zhao, J.-H. Park, K. T. Law, H. Berger, L. Forró, J. Shan, and K. F. Mak, Nature Physics **12**, 139 (2016).
[33] J. M. Lu, O. Zheliuk, I. Leermakers, N. F. Q. Yuan, U. Zeitler, K. T. Law, and J. T. Ye, Science **350**, 1353 (2015).
[34] T. Li, S. Jiang, B. Shen, Y. Zhang, L. Li, T. Devakul, K. Watanabe, T. Taniguchi, L. Fu, J. Shan, and K. F. Mak, arXiv e-prints , arXiv:2107.01796 (2021), arXiv:2107.01796 [cond-mat.mes-hall] .
[35] C. L. Kane and E. J. Mele, Phys. Rev. Lett. **95**, 226801 (2005).
[36] N. N. T. Nam and M. Koshino, Phys. Rev. B **96**, 075311 (2017).
[37] H. Shi, Z. Zhan, Z. Qi, K. Huang, E. v. Veen, J. Á. Silva-Guillén, R. Zhang, P. Li, K. Xie, H. Ji, M. I. Katsnelson, S. Yuan, S. Qin, and Z. Zhang, Nature Communications **11**, 371 (2020).
[38] V. V. Enaldiev, V. Zólyomi, C. Yelgel, S. J. Magorrian, and V. I. Fal'ko, Phys. Rev. Lett. **124**, 206101 (2020).
[39] I. Maity, P. K. Maiti, H. R. Krishnamurthy, and M. Jain, Phys. Rev. B **103**, L121102 (2021).
[40] S. J. Magorrian, V. V. Enaldiev, V. Zólyomi, F. Ferreira, V. I. Fal'ko, and D. A. Ruiz-Tijerina, Phys. Rev. B **104**, 125440 (2021).
[41] A. Weston, Y. Zou, V. Enaldiev, A. Summerfield, N. Clark, V. Zólyomi, A. Graham, C. Yelgel, S. Magorrian, M. Zhou, J. Zultak, D. Hopkinson, A. Barinov, T. H. Bointon, A. Kretinin, N. R. Wilson, P. H. Beton, V. I. Fal'ko, S. J. Haigh, and R. Gorbachev, Nature Nanotechnology **15**, 592 (2020).
[42] E. Li, J.-X. Hu, X. Feng, Z. Zhou, L. An, K. T. Law, N. Wang, and N. Lin, Nature Communications **12**, 5601 (2021).
[43] H. Li, S. Li, M. H. Naik, J. Xie, X. Li, J. Wang, E. Regan, D. Wang, W. Zhao, S. Zhao, S. Kahn, K. Yumigeta, M. Blei, T. Taniguchi, K. Watanabe, S. Tongay, A. Zettl, S. G. Louie, F. Wang, and M. F. Crommie, Nature Materials **20**, 945 (2021).
[44] N. Mounet, M. Gibertini, P. Schwaller, D. Campi, A. Merkys, A. Marrazzo, T. Sohier, I. E. Castelli, A. Cepellotti, G. Pizzi, and N. Marzari, Nature Nanotechnology **13**, 246 (2018).
[45] L. Meckbach, J. Hader, U. Huttner, J. Neuhaus, J. T. Steiner, T. Stroucken, J. V. Moloney, and S. W. Koch, Phys. Rev. B **101**, 075401 (2020).
[46] M. Li, M. Z. Bellus, J. Dai, L. Ma, X. Li, H. Zhao, and X. C. Zeng, Nanotechnology **29**, 335203 (2018).
[47] See supplementary Material for (1) Spinless time-reversal symmetry and the vanishing of Chern number; (2) Derivation of effective Hamiltonian through the perturbation theory; (3) Coulomb interaction and Hartree-Fock calculations; (4) Details for numerical calculations; (5) Effective tight-binding model calculation with lattice relaxation for moiré heterobilayer TMDs, which includes the Refs. [48–53].
[48] M. A. Cazalilla, H. Ochoa, and F. Guinea, Phys. Rev. Lett. **113**, 077201 (2014).
[49] G.-B. Liu, W.-Y. Shan, Y. Yao, W. Yao, and D. Xiao, Phys. Rev. B **88**, 085433 (2013).
[50] T. Fukui, Y. Hatsugai, and H. Suzuki, Journal of the Physical Society of Japan **74**, 1674 (2005).
[51] M. Vozmediano, M. Katsnelson, and F. Guinea, Physics Reports **496**, 109 (2010).
[52] S. Fang, S. Carr, M. A. Cazalilla, and E. Kaxiras, Phys. Rev. B **98**, 075106 (2018).
[53] B. T. Zhou, C.-P. Zhang, and K. Law, Phys. Rev. Applied **13**, 024053 (2020).
[54] J. Mao, S. P. Milovanovic, M. Andelkovic, X. Lai, Y. Cao, K. Watanabe, T. Taniguchi, L. Covaci, F. M. Peeters, A. K. Geim, Y. Jiang, and E. Y. Andrei, Nature **584**, 215 (2020).
[55] Y. Zhang, T. Devakul, and L. Fu, Proceedings of the National Academy of Sciences **118** (2021).
[56] F. D. M. Haldane, Phys. Rev. Lett. **61**, 2015 (1988).
[57] N. Levy, S. A. Burke, K. L. Meaker, M. Panlasigui, A. Zettl, F. Guinea, A. H. C. Neto, and M. F. Crommie, Science **329**, 544 (2010).
[58] F. Guinea, M. I. Katsnelson, and A. K. Geim, Nature Physics **6**, 30 (2010).
[59] J. Liu and X. Dai, Phys. Rev. B **103**, 035427 (2021).
[60] P. Stepanov, I. Das, X. Lu, A. Fahimniya, K. Watanabe, T. Taniguchi, F. H. L. Koppens, J. Lischner, L. Levitov, and D. K. Efetov, Nature **583**, 375 (2020).
[61] Y.-H. Zhang, D. Mao, Y. Cao, P. Jarillo-Herrero, and T. Senthil, Phys. Rev. B **99**, 075127 (2019).
[62] J. Y. Lee, E. Khalaf, S. Liu, X. Liu, Z. Hao, P. Kim,

and A. Vishwanath, Nature Communications **10**, 5333 (2019).
[63] M. Xie and A. H. MacDonald, Phys. Rev. Lett. **124**, 097601 (2020).
[64] C. Repellin, Z. Dong, Y.-H. Zhang, and T. Senthil, Phys. Rev. Lett. **124**, 187601 (2020).
[65] G. Chen, A. L. Sharpe, E. J. Fox, Y.-H. Zhang, S. Wang, L. Jiang, B. Lyu, H. Li, K. Watanabe, T. Taniguchi, Z. Shi, T. Senthil, D. Goldhaber-Gordon, Y. Zhang, and F. Wang, Nature **579**, 56 (2020).
[66] Y.-H. Zhang, D. Mao, and T. Senthil, Phys. Rev. Research **1**, 033126 (2019).
[67] N. Bultinck, S. Chatterjee, and M. P. Zaletel, Phys. Rev. Lett. **124**, 166601 (2020).
[68] D. Zhai and W. Yao, Phys. Rev. Materials **4**, 094002 (2020).
[69] E. J. Bergholtz and Z. Liu, International Journal of Modern Physics B **27**, 1330017 (2013).
[70] A. Abouelkomsan, Z. Liu, and E. J. Bergholtz, Phys. Rev. Lett. **124**, 106803 (2020).
[71] P. J. Ledwith, G. Tarnopolsky, E. Khalaf, and A. Vishwanath, Phys. Rev. Research **2**, 023237 (2020).
[72] C. Repellin and T. Senthil, Phys. Rev. Research **2**, 023238 (2020).